High Resolution Computation of the Aerodynamics and Acoustics of Blade Vortex Interaction

Alasdair Thom *
and
Karthikeyan Duraisamy †

Rotor Aeromechanics Laboratory
Department of Aerospace Engineering
University of Glasgow, Glasgow, G12 8QQ, United Kingdom

In the present work, high resolution CFD simulations have been performed on an idealised problem of the interaction of an independently generated vortex with a rotor blade, including a case where the vortex directly impacts on the blade. The resulting blade pressures and acoustics are comprehensively compared against experimental measurements. Two different modelling approaches are used: the first is to impose the vortex as a perturbation to the velocity field, and the second is to fully resolve the vortex formation, evolution and its interaction with the blade. For a case in which the vortex passes near the blade surface, the the fully resolved approach is confirmed to accurately preserve the vortex structure. The far field acoustic predictions offered by the fully resolved approach are seen to be very accurate and definite improvements are observed in the computed blade pressures and acoustics over the imposed vortex approach and other similar works in the literature. For a case in which the vortex axis passes through the blade, the shape and width of the acoustic pulse in the far field is accurately represented by the fully resolved approach, while the magnitude is slightly underpredicted. The improvement in prediction offered by the fully resolved approach is because this method allows for a more realistic representation of phenomena, such as dynamic change in vortex structure and trajectory due to the blade passage, that become important when the vortex miss-distance becomes small.

Nomenclature

C_T	rotor thrust coefficient, $T/\rho_\infty \pi R^2 U_{tip}^2$
U	local sectional velocity
U_∞	freestream velocity
U_{tip}	rotor tip speed
u, v, w	velocity components in x,y,z respectively
x	streamwise direction, origin at rotor hub
y	lateral direction, origin at rotor hub
z	vertical direction, origin at rotor hub
C_l	sectional lift coefficient, $L/\frac{1}{2}\rho_\infty c U_{tip}^2$
C_p	pressure coefficient $(P-P_\infty)/\frac{1}{2}\rho U_{tip}^2$
z_v	vortex/blade miss distance
p	local pressure
p_∞	freestream pressure
R	rotor radius
r	local rotor radius
c	chord
ρ	density
ψ	rotor azimuth
V_θ	swirl velocity of vortex
$CFD-FV$	CFD using field velocity approach
$CFD-R$	CFD using fully resolved approach

* athom@aero.gla.ac.uk, Postgraduate Research Student
† dkarthik@eng.gla.ac.uk, Lecturer of CFD

Background

Modern helicopter designers are faced with noise regulations that are driven by ever more stringent civilian and military requirements. A major source of rotorcraft noise comes from the rotor blades interacting with the vortices trailed from the preceding blades. This blade-vortex interaction (BVI) generates high amplitude impulsive noise that is particularly intense under certain flight conditions such as low speed descent and manoeuvre where the proximity of the trailed vortices induces rapid changes in loads on the rotor blades. BVI noise is especially important because it is known to propagate out-of-plane of the rotor and towards the ground (1), and is in a frequency range to which the human ear is highly receptive. If helicopter designers are to devise methods to reduce BVI noise, the associated physical mechanisms need to be well understood: while the passing vortices cause pressure fluctuations on the rotor blades, the structure and trajectory of the vortices will change, thus dynamically affecting the nature and intensity of the interaction. Therefore, a predictive tool should be able to represent such complicated flow phenomena if it is to be successfully used in design. In this work, the predictive capabilities of a high resolution computational fluid dynamic solver are evaluated in detail for a model BVI problem and the associated blade pressures, vortex deformation and acoustics are studied.

Over the past few decades, BVI has been the focus of both experimental and theoretical research. Experimental work has ranged from acoustic data obtained from a "quiet" aircraft flying in formation with a helicopter and measuring the noise generated (2) to experiments involving a single vortex interacting with a rotor (3). A recent example of an experimental study involving model rotor configurations is the HART tests (4, 5). These tests were performed on a Mach-scaled Bo-105 rotor and the blade loads, wake velocities and noise were measured over a range of descending flight conditions. Despite the complexities of a full rotor, much work has gone into simulating such a case. A prime example is the work of Lim *et al.*, (6) in which a grid of 108 million points was used to resolve the flow over a helicopter rotor in descending flight using a Reynolds-averaged Navier-Stokes (RANS) code coupled to a structural dynamics code. Though the agreement of the computed airloads and acoustics with experimental measurements is encouraging and an improvement compared to that from low order models, several discrepancies still exist, some of which are attributed to numerical dissipation error. For instance, the mesh size in the finest region of the wake was 5% of the blade chord, whereas previous work (7, 8) has indicated that the resolutions need to be at least six times finer in each coordinate direction. Additional difficulties in evaluating the predictive methodology resulted from uncertainties in blade structural properties and deformations. In order to develop confidence in such simulations, it must first be ensured that the relevant flow physics is sufficiently well represented. Therefore, the need to make *detailed* and *comprehensive* evaluations of the flow solver on simpler flow configurations is paramount.

A fundamental investigation into BVI was carried out by Caradonna *et al.* (3). Here a "free vortex" approach, where the vortex is generated by a fixed wing placed upstream of the rotor is employed. This vortex convects downstream to the rotor which is operated at zero thrust to minimise the creation of its own vortices. This approach significantly reduces the complexity of the problem while retaining the key features of the BVI problem as the parameters of vortex position and strength are relatively well known. The rotor was also stiffened to minimise any blade flapping such that structural dynamic effects are isolated. The simplicity of this experiment makes it ideal for validating the computational prediction of blade pressures and acoustics.

Caradonna *et al.* (9) summarise results from a variety of computational methods used to simulate the aforementioned experiment for a case in which the vortex passes close to the blade. The evaluated methods ranged from relatively simple indicial models (10), to potential flow models (11), to full computational fluid dynamic (CFD) Euler/Navier-Stokes models. Although the lower order models capture the basic trends, the CFD methods naturally capture more detail, but do not offer significantly improved predictions. Baeder and Srinivasan (12) used a three dimensional inviscid CFD approach where the vortex was imposed in the solution as a perturbation from a standard vortex model using a vortex fitting method. From this, the surface pressures and acoustics for the near-field microphone locations were calculated for cases with various vortex miss distances. This work was later extended to investigate basic parameters of BVI such as vortex strength and sense, and miss distance (13). Good agreement in blade surface pressures was noted between the experiment and CFD, thus demonstrating the feasibility of using such high fidelity methods for BVI analysis. Full CFD simulations have also been carried out by Strawn *et al.* (14) where a similar method was use to impose the vortex and the acoustics were predicted in the far-field using the Kirchhoff method (15). The work showed very promising acoustic results in the far-field when compared to experimental data. However, an exaggerated undershoot was noticed in the computations of the acoustic pulse, which was traced back to errors resulting from the imposed vortex model, as the deformation and distortion of the vortex structure were not modelled. Experimental results also showed that the vortex was not fully rolled up when it reached the rotor. Further, none of these works attempted to model the case in which the vortex directly passes through the rotor blade. Such a case is of prime importance as it generates the most intense BVI effects and also presents a greater computational challenge than other cases as the dynamic distortion of the vortex will be expectedly large.

The objective of this paper is to simulate the experiments of Caradonna *et al.* in detail. The generation, convection and interaction of the vortex is fully resolved. Using such a fully resolved approach allows for a realistic representation of the vortex structure (which may or may not be completely rolled up). Further, the vortex structure and trajectory can deform. The blade pressures and acoustic predictions will be evaluated in detail against the experiments and the standard approach of imposing the vortex. A case of zero miss distance where the vortex directly impacts on the blade is then simulated. By fully resolving the vortex, it is expected that the BVI events will be more realistically represented as it will allow the vortex to deform with the influence of the blade passage.

Details of the Experiment

The experiments of Caradonna and Kitaplioglu (3) are used to validate the key results of the present study. The objective of their work was to recreate the blade pressures and acoustics of parallel unsteady BVI in an isolated framework. The interacting vortex was generated independently by a fixed NACA 0015 wing placed upstream of a two-bladed NACA 0012 rotor. The position and angle of attack of the vortex generator could be controlled to adjust the strength and miss distance (z_v/c) of the vortex. The vortex convects downstream to the rotor where it is roughly aligned to be parallel with the quarter chord location of the rotor blade when the blade is at an azimuth of 180°. The experimental setup is shown in Fig. 1. The rotor was operated at a tip Mach number of 0.715 and at zero collective pitch to reduce the effect of interaction with its own vortices. The rotor was also stiffened in

bending and torsion to isolate aeroelastic effects. Pressure measurements were obtained along three radial locations $(r/R = 0.76, 0.88, 0.96)$ on the upper and lower surfaces of the blades. The wind tunnel walls were acoustically treated to minimise noise reflection, and acoustic data was sampled from seven microphone locations: two in the near-field directly underneath the rotor, where the primary BVI event occurs and five in the far-field. The microphone positions are summarised in table 1.

Microphone	x	y	z
1	0	-2.81	-1.42
2	0	-2.81	-1.75
3	0	-2.81	-2.12
4	0	-2.81	-2.61
5	0	-2.81	-3.01
6	-0.88	-0.24	-0.28
7	-0.88	-0.05	-0.28

Table 1: *Microphone positions relative to the rotor hub measured in rotor radii. Coordinate system origin on rotor hub. For coordinate orientation refer to Fig. 1.*

Computational Methodology

Aerodynamics

The code CHRONoS (Compressible High Resolution Overset mesh Navier-StOkes Solver) (16) is used in the present simulations. The methodology uses a vertex-centered finite volume solution on structured overset meshes. Fifth order accurate upwind Spatial discretisation is performed using using the Weighted Essentially Non-oscillatory scheme. Second order accurate implicit time integration is accomplished using the Backwards Differencing Scheme. As the flow remains attached to blade and the most dominant effects are inviscid, the code is employed in the Euler mode. The use of such an inviscid approximation is considered a first step in the study of this problem as it is easier to ascertain numerical dissipation effects. In order to serve as a basis for comparison and to relate the present results to previous work, two different approaches were used:

Field velocity approach: This method is similar to the vortex fitting method of Srinivasan 12 where the effect of the trailed vortex from the vortex generator is imposed in the solution as a perturbation of the field velocity. A Scully model is assumed for the vortex with the circulation and the core radius values taken from experimentally measured data from a related fixed wing experiment (17). The tangential velocity equation for the standard model is expressed in dimensionless form as:

$$V_\theta(r) = \frac{\Gamma}{2\pi} \frac{r}{(r_c^2 + r^2)}$$

Where the vortex circulation and core radius are $\Gamma = 1.12 U_\infty c$ and $r_c = 0.162c$, respectively. The near-blade domain is discretised using a body conforming mesh of C-O topology with dimensions $229 \times 71 \times 63$ cells in the chordwise, radial and wall normal directions, respectively. This mesh is overset inside a cylindrical background mesh of dimensions $147 \times 101 \times 73$ in the azimuthal, radial and vertical directions, respectively. A hole of constant topology is cut in the rigidly rotating background mesh in the region surrounding the blade mesh. 720 time steps per revolution (with 5–10 sub-iterations per time step) were used to ensure time accuracy and convergence of the calculation. Both the background and blade meshes are rigidly rotated.

This method provides an intermediate step between a fully resolved CFD simulation of the problem and other lower order models. By representing the vortex using a standard model, considerable computational time and effort can be saved as the vortex position and strength can be specified and the vortex structure does not have to be resolved and preserved in the solution domain. However, as mentioned earlier, this method has limitations as it produces a symmetrical vortex with a profile that is of constant strength. In the experimental work (3) it was noted that the vortex strength severely deteriorated due to the vortex being disrupted by the blade passage and particularly as the vortex impinges on the rotor hub assembly. This deformation of the vortex due to the passing of the blade becomes more significant as the miss distance is decreased. Furthermore, the vortex was determined to be not fully rolled up when it reached the rotor and would therefore have a different profile from the assumed model. As a result of these limitations, this method cannot be used to accurately simulate cases with small or zero miss distances.

Resolved vortex approach: In this approach, the generation of the vortex, its convection and interaction with the rotor blade is fully resolved, thus providing a more physically realistic representation of the vortex. A three mesh overset system for the vortex generator, wind tunnel and rotor blade is used as shown in Fig. 1. The wind tunnel and the vortex generator meshes remain stationary while the rotor mesh rotates inside the wind tunnel mesh. The vortex generator and rotor blade both use a body conforming mesh of C-O topology with sizes $243 \times 119 \times 73$ and $209 \times 60 \times 51$ points in the chordwise, radial and wall normal directions, respectively. The wind tunnel is represented by a Cartesian mesh with $185 \times 134 \times 88$ points in the the downstream, cross stream and vertical directions respectively. Holes are cut in the wind tunnel mesh where the blade of the rotor and the vortex generator are located. Three fringe layers were used to interpolate information from rotor/vortex generator meshes to the boundaries of the hole in the wind tunnel mesh. The hole corresponding to the blade mesh is dynamically re-cut as the rotor rotates (Fig. 2). This is accomplished first by rotating the fringe layer of the existing hole. All points enclosed by the fringe layers are then treated as new hole points and blanked out. This dynamic hole cutting is performed every time step and new donor points and interpolation factors are found using a stencil walking procedure (18).

This case is first run keeping the rotor stationary until a steady solution is reached. The vortex generator (which is set at an angle of attack of 12°) generates a vortex that con-

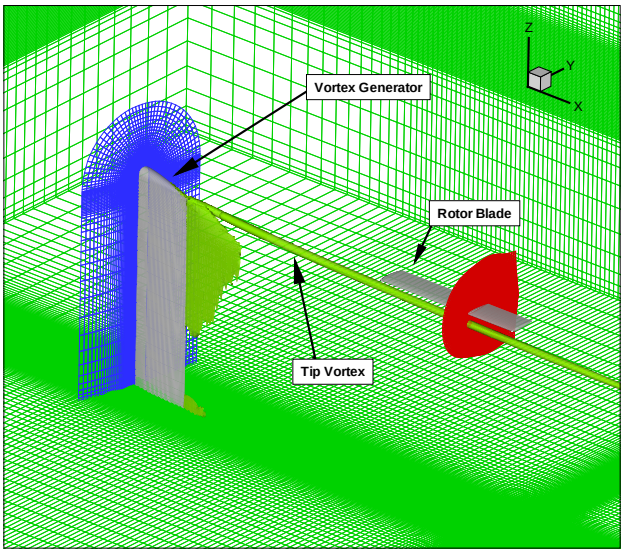

Figure 1: *Mesh used in the fully resolved approach. Sample planes are shown from rotor, vortex generator and wind tunnel meshes. Rotor blade at* 180°

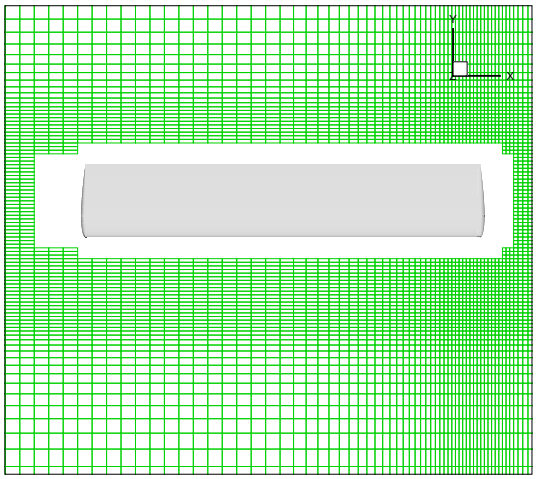

(a) *Original blade mesh position*

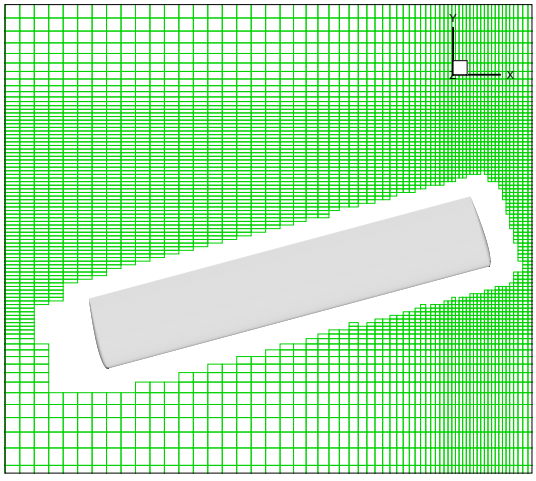

(b) *Blade rotated by* 25°

Figure 2: *Sample plane of background mesh.*

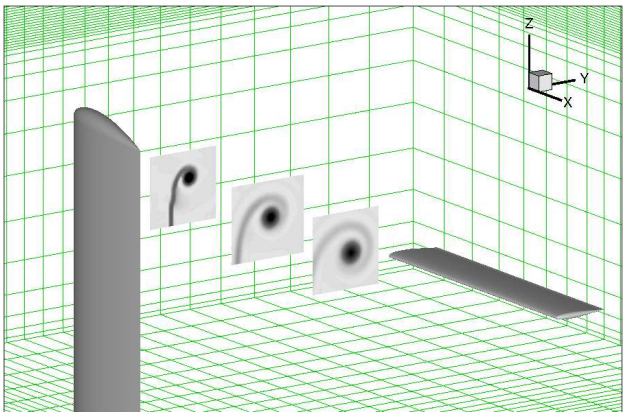

Figure 3: *Vorticity slices in background mesh as vortex convects towards the rotor.*

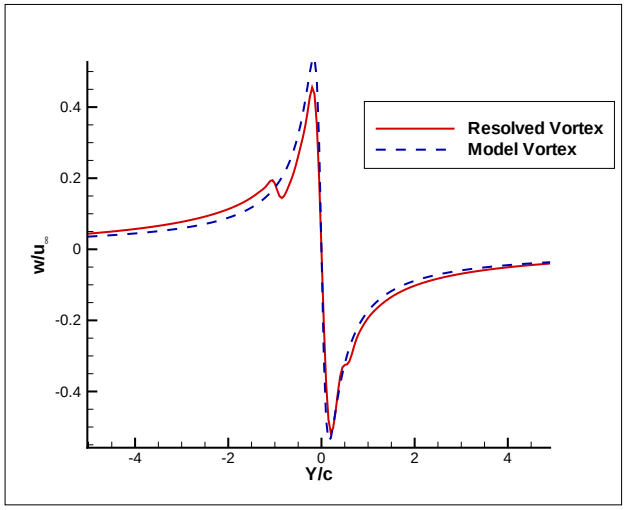

Figure 4: *Comparison of vortex vertical velocity between the resolved approach and Scully model at* $\frac{r}{R} = 0.88$.

vects approximately 8 chord lengths through the solution before it reaches the rotor. It is therefore important that the vortex structure is preserved as it moves through the solution and is not dissipated due to numerical error. This is achieved by the use of the efficient numerical scheme and by clustering points in all three meshes where vorticity is present in the solution. At least 8 mesh points were ensured across the vortex core in order to reduce numerical dissipation. The use of a fifth-order accurate upwind numerical scheme is found to preserve the vortex strength as it convects towards the rotor and Fig. 3 shows the vortex evolving as it convects towards the rotor. It was confirmed that the dissipation of the peak-to-peak velocity of the vortex was negligible. From the detailed experiments of McAlister *et al.* (17) the computed vortex profile is found to closely agree with a model that correlated well with the experimental results (Fig. 4).

Once a steady vortex has formed in the solution, the blade mesh is rotated at the rate of 0.5° per time step (with 5 sub-iterations per time step). The solution is allowed to complete three and a half rotor rotations with data being collected over the last revolution. As the blade mesh ap-

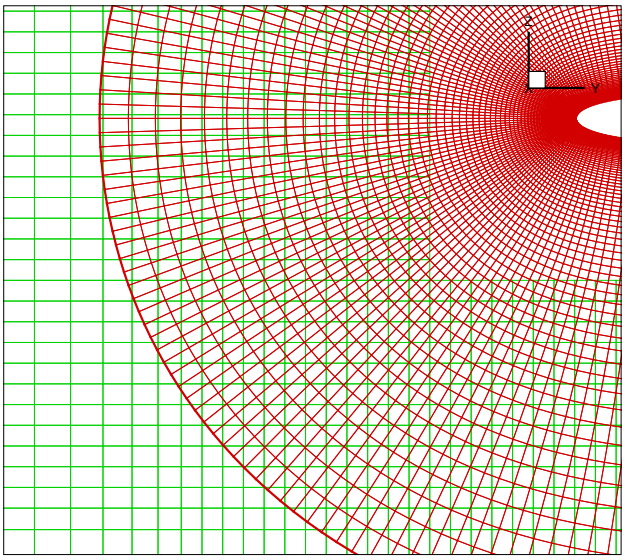

Figure 5: *Sample overlapping planes of the background and rotor meshes.*

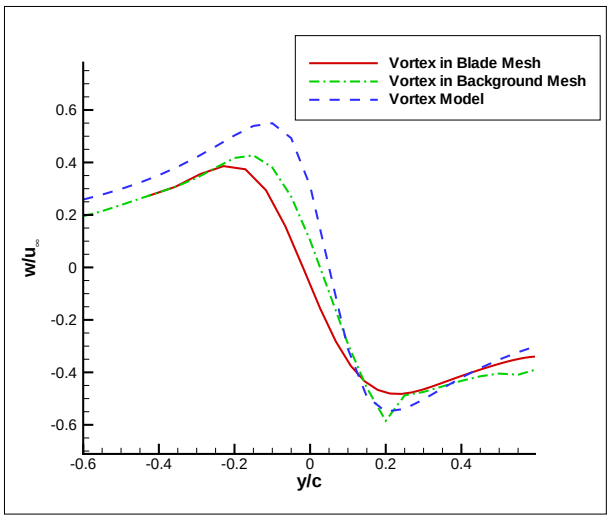

Figure 6: *Vertical velocity of the vortex in the wind tunnel and blade mesh in the overlap region. Vortex model profile is also shown for comparison.*

proaches the vortex, it is ensured that the spacing in both meshes matched to minimise data transfer errors. Fig. 5 shows a section of the fine spacing used in the region of the mesh where the vortex passes from the background mesh to the blade mesh. Several meshes of different outer boundary spacings were tested to evaluate their effectiveness at interpolating information between grids. Fig. 6 shows a comparison of the velocity profile of the vortex as determined from the wind tunnel and blade meshes at an azimuth of 171.5°. The undistorted model vortex is also plotted as a reference.

Indicial Model

A third approach to model the Caradonna and Kitaplioglu experiment used a simple indicial model. This approach accounts for the downwash on the blade caused by the shed vorticity by a numerical approximation to Wagner's function. The indicial model gives an effective sectional angle of attack, from which the sectional lift is calculated using empirical two dimensional incompressible data for a NACA 0012 aerofoil. This lift was modified using the Prandtl-Glauret compressibility correction. The induced velocity field of the vortex is represented using the Scully model as used in the field velocity approach. This simple model is used as a baseline case to verify and compare with the more complicated CFD methods. It is also important to evaluate the accuracy of such simple models which are many orders of magnitude less expensive than the full CFD method. Each blade section is assumed to be independent of the others and hence three dimensional effects are ignored.

Acoustic modelling

In theory, acoustic pressures can be computed directly from a CFD solution by using highly refined meshes over the whole solution domain. This method has been shown to be feasible for near field pressure calculations where the solution is well resolved. However, resolving the acoustics directly as the waves propagate to the far-field becomes computationally expensive and subject to numerical errors as the acoustic waves are linear, and hence, prone to dissipation errors. In the present work, the acoustics in both the near and far field is computed using the Farassat-1A on-surface formulation of the Ffowcs Williams-Hawkings equation (19). This formulation is widely used in rotor acoustic calculations, mainly because of the efficiency that results from the analytic representation of the derivatives in source time. The surface pressures from the CFD solution are used in the acoustics solver. In the present approach, the loading and thickness sources are represented, while the noise resulting from the quadrupole sources is neglected.

For the indicial model, the aerodynamic force contributed by each blade panel is used to construct a point acoustic source at the quarter chord point of the blade. Integration of the sound radiated by each of these sources represents the loading noise. The thickness noise is modelled independently by attaching a source-sink pair to each blade section. Noise due to quadrupole terms is also neglected in this method.

$\frac{1}{4}$ Chord Miss Distance Simulations

Blade Loads

The methodologies were evaluated for a case of parallel BVI where the blade misses the vortex by 0.25 chords ($z_v/c = -0.25$). The thrust response to a parallel BVI is characterised by the abrupt change in loading on the blade as it passes over the vortex. In this case, two separate BVIs occur: a strong primary pulse at an azimuthal location of approximately 180° (when the rotor blade is upstream of

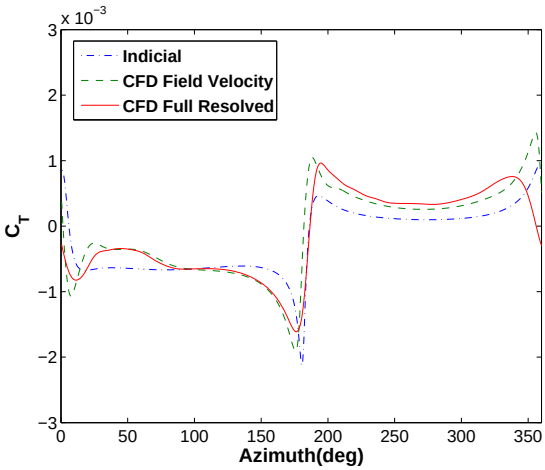

Figure 7: *Thrust response over one rotor revolution. Primary BVI occurs at* $\psi \approx 180^\circ$*, downstream BVI occurs at* $\psi \approx 0^\circ$

the hub) and a weaker downstream BVI at an azimuth of approximately 0° (when the rotor blade is downstream). Fig. 7 shows the thrust response of the rotor for one full revolution as given by the various computational methods. All three methods capture the characteristic response and magnitude of the BVI pulse. At the downstream BVI, the magnitude of the pulse is significantly greater for both the indicial and field velocity approaches compared to the fully resolved approach. This difference occurs as the vortex in the fully resolved approach reduces in strength, whereas in the other two methods, the vortex strength is modelled as a constant. This vortex diffusion occurs for two reasons in the fully resolved case: Firstly, because the primary interaction with the rotor changes the profile of the vortex. Secondly, because the streamwise spacing in the background mesh is rapidly increased downstream of the centre of the rotor rotation. This increase in mesh spacing is deliberately done with the intention of diffusing the vortex, as in the experiment (3) the vortex was shown to rapidly diffuse (and eventually burst) on interaction with the rotor hub assembly. Because the rotor hub has not been modelled here, it is felt that the artificial diffusion of the vortex is justified in the present work. This results in the vortex losing strength as it convects past the rotor and reduces the strength of the downstream BVI which is not of interest here. Also, as will be shown, if this vortex is not diffused, the secondary BVI can corrupt the acoustic results.

Similar results can be seen in the plot of the rotor sectional C_l around the azimuth (Fig. 8). The lack of modelling any three dimensional effects can be seen in the indicial case as the magnitude of the C_l increases towards the tip and is much greater than the CFD methods. The field velocity approach also shows a more concise BVI event, with the pulse contours being restricted to a region close to an azimuth of 180°. This is in contrast to the fully resolved vortex approach where the effects of the BVI are smeared over a greater azimuth range. This difference arises from the interaction that occurs between the blade and the vortex

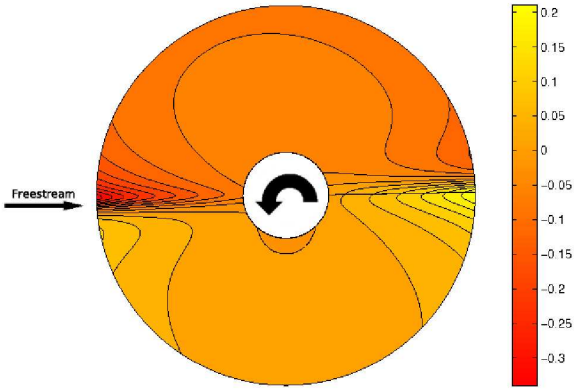

(a) *Indicial Model*

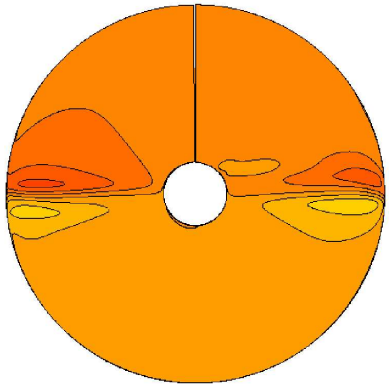

(b) *CFD-Field Velocity*

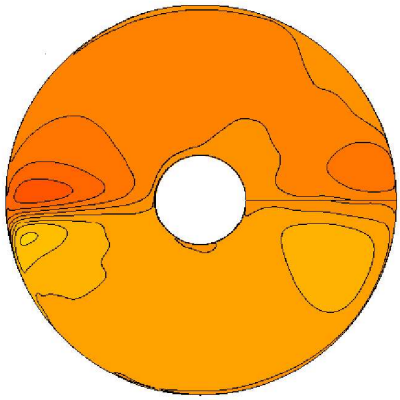

(c) *CFD-Resolved*

Figure 8: *Sectional* C_l *over one rotor revolution. Primary BVI occurs to the left.*

that manifests itself as a less distinct BVI. This effect will be further discussed in the section on flow visualisation.

Surface Pressure Coefficient

The difference in pressure coefficient between the upper and lower surfaces of the blade at various chordwise locations at $r/R = 0.88$ for both CFD methods and the experimental results is shown in Fig. 9. Plotting the difference in pressure removes the steady effects and isolates the BVI event. The greatest fluctuations in pressure can be found at the outboard sections of the blade because of the higher speeds near the tip. Fig. 9 shows that the general characteristic shape of the BVI pulse is captured here by both the field velocity and the fully resolved approach. The CFD results have both been phased to match the experimental peak pressures. This phasing is justified by the fact that in the experimental work, the exact vortex location at the interaction was not known and an azimuth error of $\pm 4^\circ$ was reported. The magnitude of the pressure pulse closely matches the experimental data especially at the leading edge location (Fig. 9(a)) where the pressure pulse is approximately 6 times greater than at locations towards the trailing edge. As the majority of the fluctuation is at the leading edge of the aerofoil, this region is the most important to capture and will have the greatest influence on the acoustics. Towards the trailing edge, the pressure response of the fully resolved case begins to differ from the experimental and field velocity results (Fig. 9(g) - 9(i)). The experiment shows the width of the BVI pulse as being more concise towards the trailing edge which is represented well by the field velocity approach. In the fully resolved approach, the BVI event occurs over a larger azimuth range, suggesting that the vortex is deforming and stretching over a greater range than what occurs physically. However, this width difference is minimal and localised towards the trailing edge and thus will have less of an impact on the resulting acoustics. It has to be recognised that small changes in the vortex position and miss distance can significantly alter the location of the pressure pulses near the leading edge of the blade because of the large gradients. As the exact vortex positions are not known from the experiment, it is therefore difficult to directly compare the calculated values of the pressures against experimental results.

There are also noticeable fluctuations in the pressure at various points (Fig. 9(b) and 9(c)) which is captured in both CFD approaches. Analysis of the flowfield showed the presence of a small supersonic flow pocket on the upper surface of the aerofoil which might be missed in the experimental data because of averaging over several revolutions that may smear out the small scale fluctuations induced by this highly unsteady region. The presence of shocks are to be expected as the rotor tip encounter a maximum incident Mach number of 0.85. A survey of the local Mach numbers on the blade surface found that a maximum value of 1.2 was reached. It is also possible that the use of the viscous terms might diminish these additional fluctuations. Overall, the pressure predictions are reasonably accurate and can thus be used as a reliable input for the

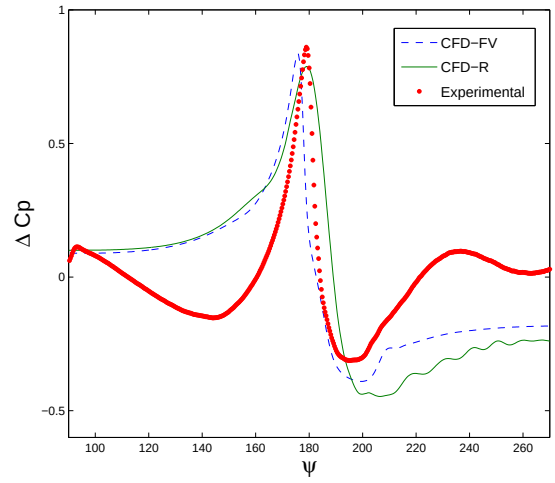

(a) $\frac{x}{c} = 0.02$

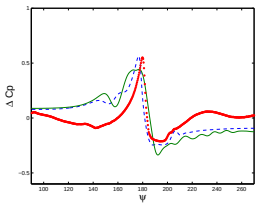

(b) $\frac{x}{c} = 0.11$

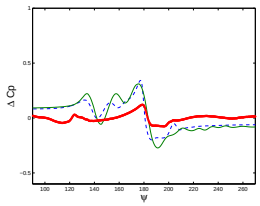

(c) $\frac{x}{c} = 0.20$

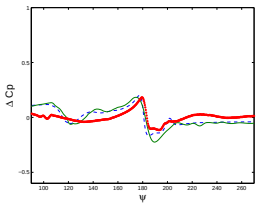

(d) $\frac{x}{c} = 0.31$

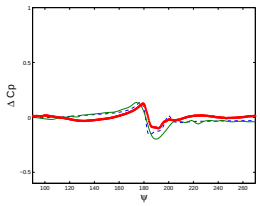

(e) $\frac{x}{c} = 0.40$

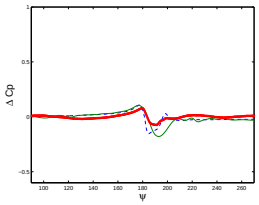

(f) $\frac{x}{c} = 0.48$

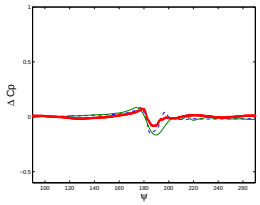

(g) $\frac{x}{c} = 0.56$

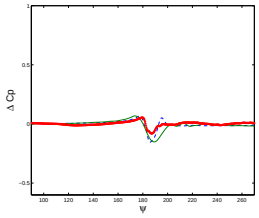

(h) $\frac{x}{c} = 0.64$

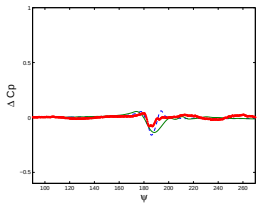

(i) $\frac{x}{c} = 0.72$

Figure 9: *Time history of the difference between the upper and lower blade surface pressure at various chord locations,* $\frac{z_v}{c} = -0.25$.

acoustic computations.

Acoustics

The pressure distribution calculated on the blade surface is used to predict the acoustic pressure in the far-field. Fig. 10 shows the predicted and measured pressures for all microphone locations at which data is available. The noise predicted from the indicial model is shown for one microphone in the far-field (Fig. 10(a)) and one microphone in the near-field (Fig. 10(b)). The resolved CFD approach is seen to predict the far-field acoustics very accurately in magnitude and characteristic shape. The acoustic predictions from the field velocity approach significantly deviates from the measured acoustics at the trailing edge of the pulse, where a significant negative dip is noticeable in the predicted sound. A similar feature of the dip has been reported previously by Strawn *et al.* (14) where a similar method to the field velocity approach was used to simulate the experiment. They reported that this dip was caused by the negative acoustic waves from the downstream BVI propagating upstream to the microphone. This feature is not present in the experimental data and the fully resolved case due to the vortex diffusing before the downstream BVI event occurs (and in the indicial model where the downstream BVI is ignored), whereas in the field velocity approach, the vortex strength is constant at both BVI locations. Presently, additional acoustic calculations were performed assuming a single bladed rotor, thus only one BVI event occurs at a given time. In these calculations, it was confirmed that the downstream BVI did indeed contribute to the negative pulse.

The near-field acoustics are presented in Fig. 10(b) and 10(f). Unlike the far-field results, the near-field acoustics are not as accurate. This difference may arise from the on-surface approximation and also from the influence of the additional non-linearities that are not represented in the formulation. Also, quadrupole sources are neglected in this analysis and these may not be negligible in the near-field. The simulations of McCluer (13) were able to resolve the acoustic pressure in the near-field directly from the CFD flow solution and good agreement was seen in their results.

The indicial acoustic response captures the amplitude of the pulse well. However, the pulse width is much narrower than the other methods use and this is to be expected as the airfoil section in the indicial model is represented as a compact source.

Overall, the acoustic prediction given by the resolved CFD method is consistently better than that predicted by the field velocity approach and the far-field predictions prove to be an improvement over previously published work.

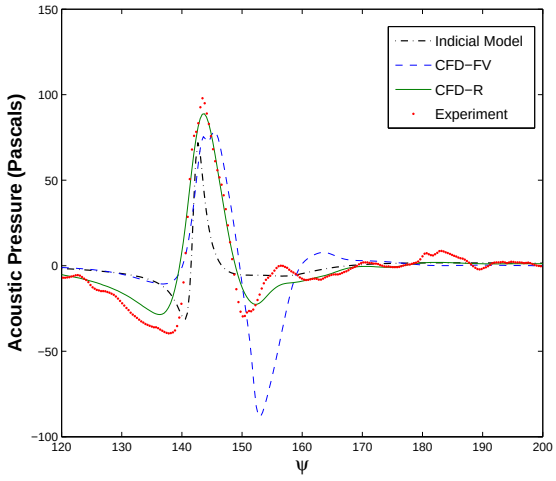

(a) *Microphone 3*

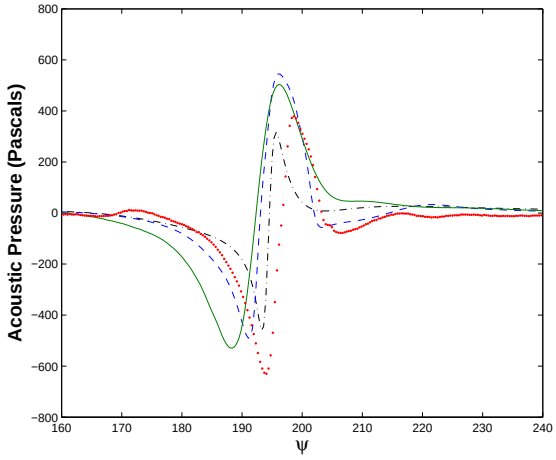

(b) *Microphone 6*

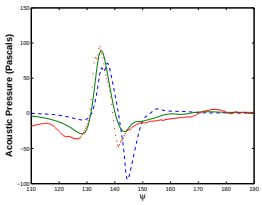

(c) *Microphone 2*

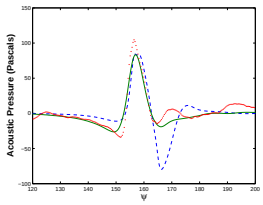

(d) *Microphone 4*

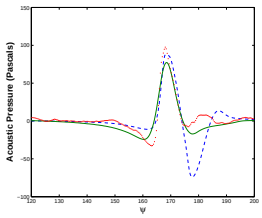

(e) *Microphone 5*

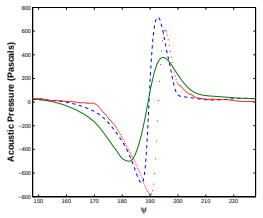

(f) *Microphone 7*

Figure 10: *Acoustic pressure predictions at various microphone locations compared to experiment. Near-field microphones 6 - 7, far-field microphones 2 - 5.* $\frac{z_v}{c} = -0.25$

Direct Impact Simulations

A zero vortex miss distance case where the vortex impacts directly on the blade is now considered using the fully resolved approach. The difference in pressures between the

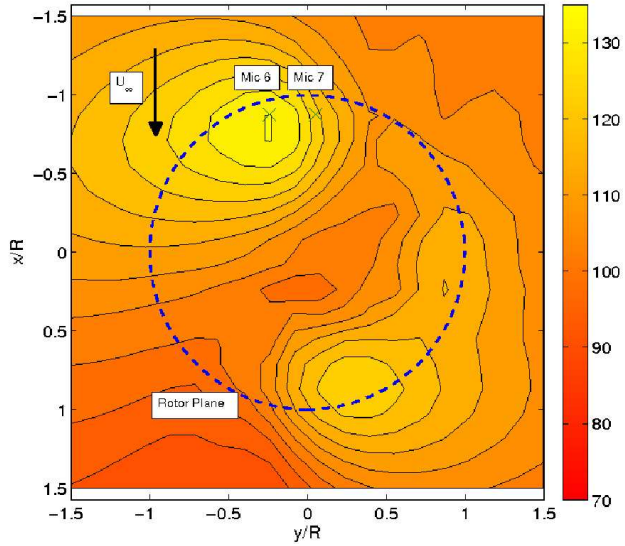

(a) *Near-fi eld Plane - 2c below rotor plane.*

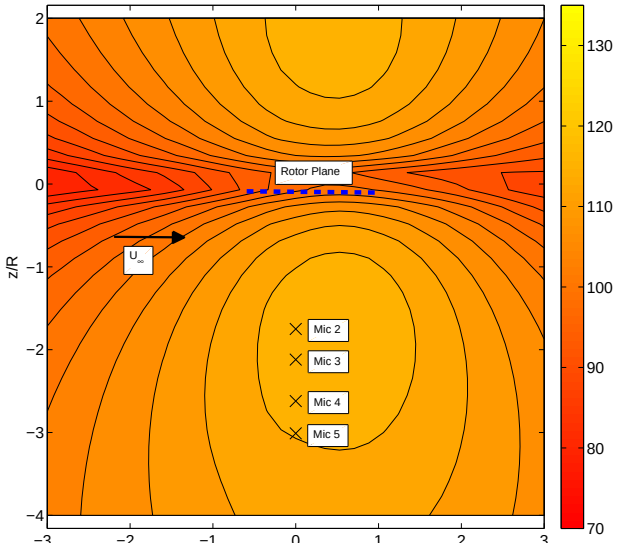

(b) *Far-fi eld Plane - 3 radii to port side of rotor plane.*

Figure 11: *Sound pressure levels in decibels over one complete rotor revolution for a plane in the near-field and the far-field.* $\frac{z_v}{c} = -0.25$

upper and lower surface for a direct impact case are shown in Fig. 12. The leading edge region pulse is captured by the fully resolved approach although its magnitude is under predicted. The pressure in other locations are also represented well, especially towards the trailing edge. As in the $z_v/c = -0.25$ case, the pressures predicted by the resolved CFD are more smeared towards the trailing edge.

The field velocity approach captures the characteristic shape of the pressure pulse but differs significantly in magnitude at the leading edge pressure point. Additional unphysical fluctuations after the main BVI pulse are also seen. These additional fluctuations are present across the chord of the aerofoil and are a direct result of the model not being physically realistic.

The acoustic predictions are shown in Fig. 13. In the far-field, the fully resolved approach is seen to predict the shape and width of the acoustic pulse well. The magnitude of the wave is under predicted, and this is consistent with the under prediction of the pressures on the blade surface. The field velocity approach shows large fluctuations in the acoustic pulse after the initial pulse. This noise comes from the additional pressure pulses on the surface of the blade which were noted previously. The near-field noise is also well under predicted compared to the resolved CFD method (Fig. 13(b)).

The results from the indicial model are also shown for a microphone in the far-field and the near-field and a severe under prediction of the magnitude is noticed, as is a very narrow pulse width. The contours of the sound pressure level are shown in Fig. 14 and show a very similar character to that in Fig. 11, but with greater magnitude of the radiated sound.

Flow Visualisation

Using the fully resolved vortex approach it is possible to visualise the vortex deformation as it interacts with the blade. Fig. 15 shows the contours of vorticity in the streamwise direction on a slice through the rotor blade for $z_v/c = -0.25$ at $r/R = 0.88$, which is the radial location at which the pressures were compared. Vorticity contours are plotted at various azimuthal locations from the vortex entering the blade grid to it leaving after the interaction. Fig. 15(a) shows the vortex before the interaction as it enters the blade grid. The vortex sheet can be seen to spiral away from the vortex core. As noted in the experimental work, the vortex is not be fully formed as it reaches the rotor (13). As the rotor approaches the vortex, the vortex begins to deform and interact with the blade. The blade passes the vortex and some of its core vorticity is entrained into the vorticity generated by the blade (as this is an inviscid method, the blade surface can be visualised as a thin vortex sheet), thus stretching the vortex. This stretching causes the pressure pulse to be wider toward the trailing edge of the aerofoil as reported earlier. As the vortex is severely distorted, this is not a true “miss distance” case, but is essentially a case of weak direct impact. It should be noted that the vortex is generated by a wing of chord

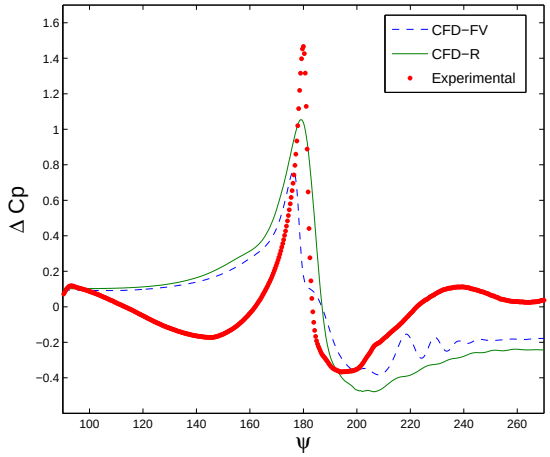

(a) $\frac{x}{c} = 0.02$

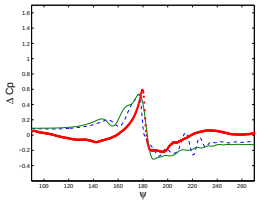

(b) $\frac{x}{c} = 0.11$

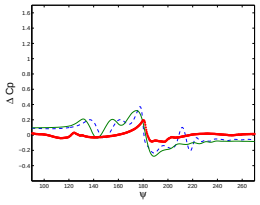

(c) $\frac{x}{c} = 0.20$

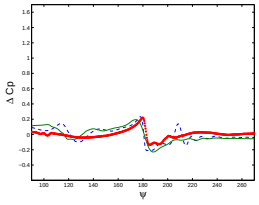

(d) $\frac{x}{c} = 0.31$

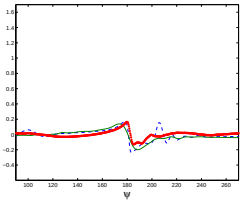

(e) $\frac{x}{c} = 0.40$

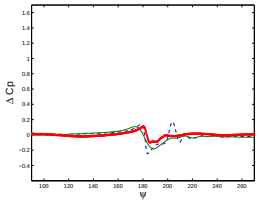

(f) $\frac{x}{c} = 0.48$

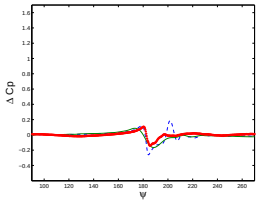

(g) $\frac{x}{c} = 0.56$

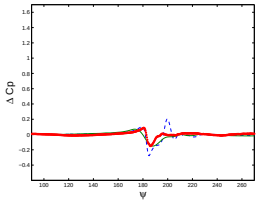

(h) $\frac{x}{c} = 0.64$

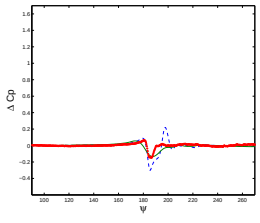

(i) $\frac{x}{c} = 0.72$

Figure 12: *Time history of the difference between the upper and lower blade surface pressures at various chord locations,* $\frac{z_v}{c} = 0$.

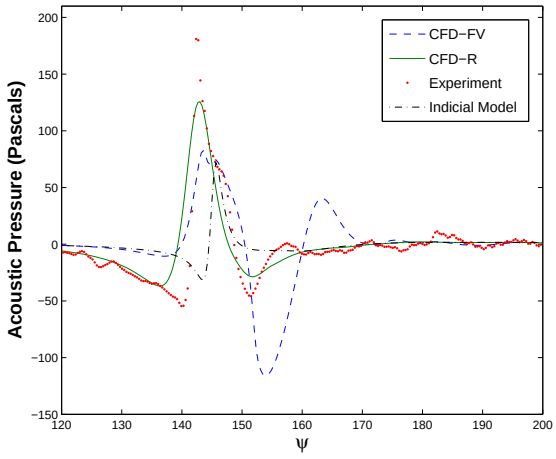

(a) *Microphone 3*

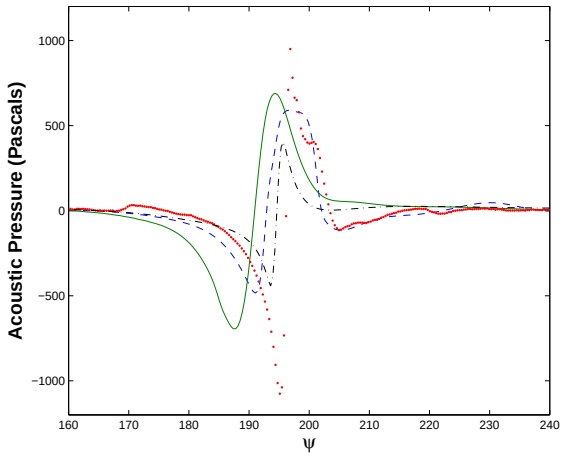

(b) *Microphone 6*

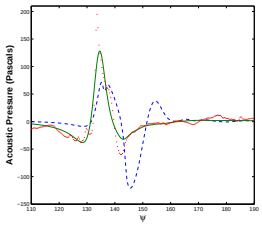

(c) *Microphone 2*

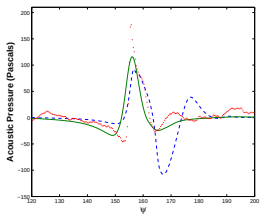

(d) *Microphone 4*

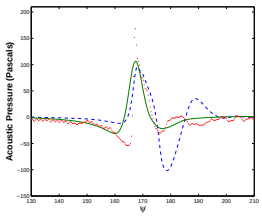

(e) *Microphone 5*

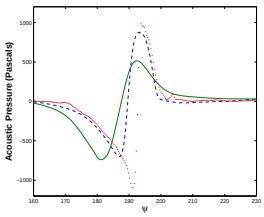

(f) *Microphone 7*

Figure 13: *Acoustic pressure predictions at various microphone locations compared to experiment. Near-field microphones 6 - 7, far-field microphones 2 - 5.* $\frac{z_v}{c} = 0$.

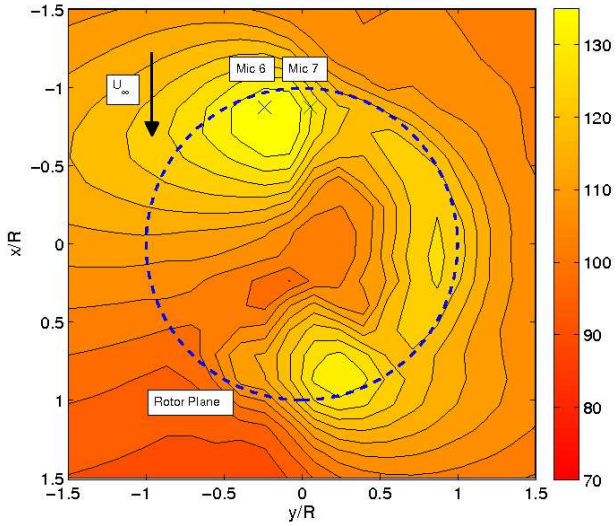

(a) *Near-fi eld Plane - 2c below rotor plane.*

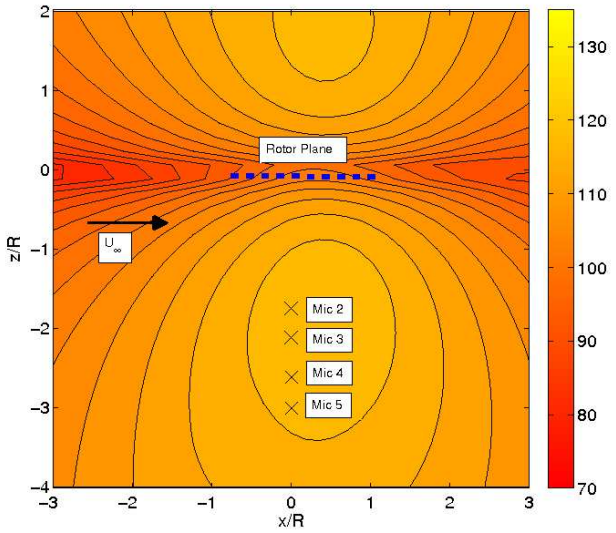

(b) *Far-fi eld Plane - 3 radii to port side of rotor plane.*

Figure 14: *Sound pressure levels in decibels over one complete rotor revolution for a plane in the near-field and the far-field.* $\frac{z_v}{c} = 0$

three times greater than the rotor blade chord. BVI that would occur on a helicopter rotor would involve a vortex generated by a rotor blade of the same chord which would generally produce a vortex with a smaller core, and therefore, a miss distance of 0.25 chords would mean that the vortex core does not interact with the blade surface.

For the direct impact case, the flow visualisation (Fig. 16) shows the blade cutting the vortex directly through its core. As the vortex approaches the blade, the core begins to compress, causing the vorticity in the vortex core to intensify as the area of the core decreases. When the vortex reaches the leading edge of the blade, the upper and lower regions of the vortex begin to stretch around the surface of the aerofoil while a significant portion of vorticity is still found at the leading edge (Fig. 16(c) and 16(d)). The core is then stretched across the blade and eventually the vortex is split as it leaves the rear of the blade grid. Although the blade appears to split the vortex structure, it is found to re-form after the interaction.

Conclusions

In this paper, the interaction of an independently generated vortex with a rotating blade was simulated using a high resolution overset mesh Euler solver. The CFD method compared a field velocity approach in which the vortex was imposed in the solution from a standard vortex model and a fully resolved approach in which the vortex formation, convection and interaction was resolved. The cases of a $0.25c$ miss distance and direct impact were analysed and the surface pressures and acoustics were compared in detail with experimental measurements.

With the use of high accuracy numerical schemes and efficiently distributed meshes, the vortex formation and convection to the rotor was accurately captured. For the $0.25c$ miss distance case, the results of the field velocity approach are similar to those published in the literature, while the resolved vortex approach showed considerably better agreement, especially in the far-field acoustic results, where the pulse shape and magnitude are extremely well predicted. For the direct impact case, the improvement offered by the resolved vortex approach is significant, primarily because of the inclusion of the effects of vortex distortion. Although the magnitude of the acoustic pulse in the far-field is under predicted, the shape characteristics are well represented.

By fully resolving the vortex and its interaction with the blade the deformation of the vortex was simulated and could be visualised. It was found that the vortex is severely distorted and entrained into the vorticity generated by the blade surface, even for the case where the vortex missed the blade by 0.25 chords. The vortex was seen to be severely distorted by the interaction and in the case of direct impact the vortex core was split by the blade. Despite this severe distortion, the vortex was seen to re-form downstream of the interaction in both cases.

The practical significance of the results of the resolved vortex approach is that this calculation is carried out in a

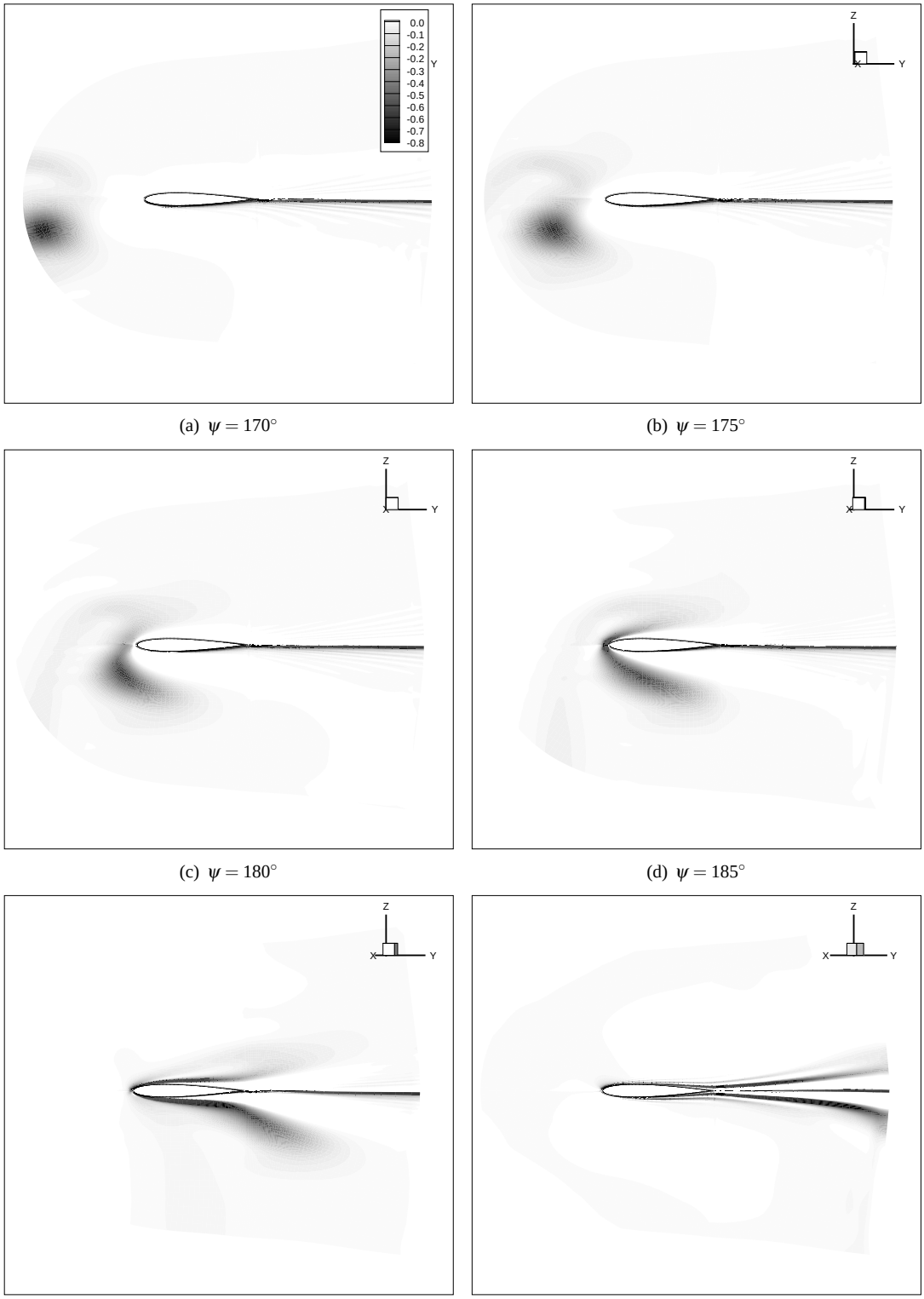

(a) $\psi = 170^\circ$ (b) $\psi = 175^\circ$

(c) $\psi = 180^\circ$ (d) $\psi = 185^\circ$

(e) $\psi = 195^\circ$ (f) $\psi = 215^\circ$

Figure 15: *Contours of streamwise vorticity at* $\frac{r}{R} = 0.88$ *in blade grid.* $\frac{z_v}{c} = -0.25$

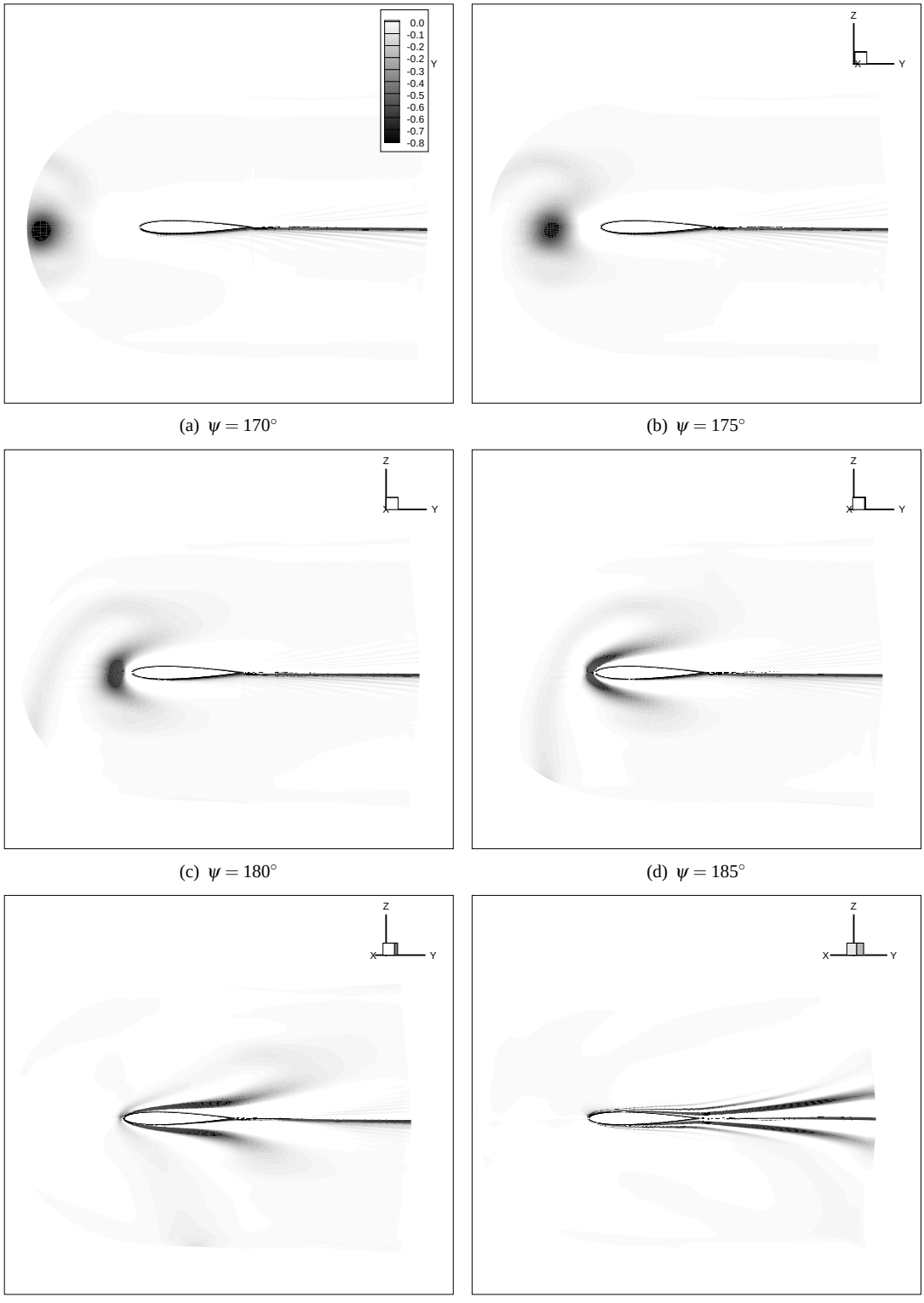

(a) $\psi = 170^\circ$ (b) $\psi = 175^\circ$

(c) $\psi = 180^\circ$ (d) $\psi = 185^\circ$

(e) $\psi = 195^\circ$ (f) $\psi = 215^\circ$

Figure 16: *Contours of streamwise vorticity at* $\frac{r}{R} = 0.88$ *in blade grid.* $\frac{z_v}{c} = 0$

generalised computational framework that is readily extendable to larger and more complex simulations on realistic rotor configurations. Future work will be focused on improving the aerodynamic modelling through the solution of the Reynolds-averaged Navier Stokes equations and the acoustic modelling by using the permeable Ffowcs Williams-Hawkings equations.

Acknowledgments

The authors would like to thank Dr. Cahit Kitaplioglu for his assistance with the experimental data and Dr. Jay Sitaraman for his help with the acoustic modelling.

References

[1]JanakiRam, R.D., "Aeroacoustics of Rotorcraft" *Aerodynamics of Rotorcraft, AGARD Report No. 781, November 1990.*

[2]Schmitz, F. H., and, Boxwell, D. A., "In flight Far-Field Measurements of Blade-Vortex Interaction Noise," *Journal of the American Helicopter Society, vol. 21, no. 4, Oct.1976, pp. 2-16.*

[3]Caradonna, F.X., Kitaplioglu, C., and, McCluer, M., "An Experimental Study of Parallel Blade-Vortex Interaction Aerodynamics and Acoustics Utilizing an Independently Generated Vortex," *NASA/TM-199208790 July 1999.*

[4]Kube,R., Splettstoesser, W. R., Wagner, W., Seelhorst, U., Yu, Y. H., Tung, C., Beaumier, P., J. Prieur, G. Rahier, P. S., Boutier, A., Brooks, T.F., Burley, C.L., Boyd, D. D., Mercker, E., and, Pengel, K., "HHC aeroacoustics rotor tests in the German-Dutch wind tunnel: Improving physical understanding and predictive codes," *Journal of Pressure Vessel Texhnology, Vol. 2, No. 3, 1998, pp. 177 - 190.*

[5]van der Wall, B., Junker, B., Burley, C., Brooks, T., Yu, Y. H., Tung, C., Raffel, M., Richard, H., Wagner, W., Mercker, E., Pengel, K., Holthusen, H., Beaumier, P. and, Delrieux, Y., "The HART 2 test in the LLF of the DNW - a Major Step towards Rotor Wake Understanding," *Proceedings of the 28th European Rotorcraft Forum, Bristol, England, 12–20 September, 2002.*

[6]Lim, J., Nygaard, T., Strawn, R., and, Potsdam, M., "BVI Airloads Prediction Using CFD/CSD Loose Coupling," *AHS Vertical Lift Aircraft Design Conference, San Francisco, CA, 18-20 January, 2006.*

[7]Duraisamy, K., and, Baeder, J., "High Resolution Wake Capturing Methodology for Hovering Rotor Simulations," *Journal of the American Helicopter Society, Vol. 52 (2) 2007.*

[8]Wake B.E., and, Choi, D."Investigation of high-order upwinded differencing for vortex convection," *AIAA journa 1996, vol. 34, no2, pp. 332-337.*

[9]Caradonna, F., Kitaplioglu, C., and, McCluer, M.,"Methods for the prediction of Blade-Vortex Interaction Noise," *American Helicopter Society Technical Specialists' Meeting for Rotorcraft Acoustics and Aerodynamics, Williamsburg, VA, October 1997.*

[10]Leishman, J.G., "Aeroacoustics of 2-D and 3-D Blade Vortex Interaction Using the Indicial Method," *American Helicopter Society 52nd Annual Forum Proceedings, Washington, D.C., June 4-6, 1996.*

[11]Bidgeman, J. O., Ramachandran, K., Caradonna, F. X., and, Prichard, D. S., "A Computational Analysis of Parallel Blade-Vortex Interactions Using Vorticity Embedding," *American Helicopter Society 50th Annual Forum Proceedings, Washington, D.C, May, 1994.*

[12]Srinivasan, G. R., "A Free-Wake Euler and Navier Stokes CFD method and its applications to Helicopter Rotors Including Dynamic Stall," *JAI Associates, Inc., JAIA-TR-93-01, Nov. 1993.*

[13]McCluer, M., "Helicopter Blade-Vortex Interaction Noise with Comparisons to CFD Calculations," *NASA Technical Memorandum 110423, December 1996.*

[14]Strawn, R.C., Oliker, L., and, Biswas, R. "New Computational Methods for the prediction and Analysis of Helicopter Acoustics," *Journal of aircraft, 1997, vol. 34, no5, pp. 665-672.*

[15]Farassat, F., and, Myers, M. K., "Extension of Kirchoff's Formula to Radiation from Moving Surfaces," *Journal of Sound and Vibration, Vol. 123, No. 3, 1988, pp. 451-460.*

[16]Duraisamy, K., and, Brown, R. E., "Aerodynamic Response of a Hovering Rotor to Ramp Changes in Pitch Input," *American Helicopter Society 64th Annual Forum Proceedings, Montreal, Canada, April 29 May 1, 2008.*

[17]McAlister, K.W., and, Takahashi, R.K., "NACA 0015 Wing Pressure and trailing Vortex Measurements," *NASA TP 3151, 1991.*

[18]Gupta, V., "Quad Tilt Rotor Simulations in Helicopter Mode using Computational Fluid Dynamics," *Ph.D. Thesis, University of Maryland, December 2005.*

[19]Brentner, K., and, Farassat, F., "Modeling Aerodynamically Generated Sound of Helicopter Rotors," *Progress in Aerospace Sciences, Vol. 39, 2003.*